HYDROLOGICAL PROCESSES
Hydrol. Process. **25**, 2071–2084 (2011)
Published online 1 February 2011 in Wiley Online Library
(wileyonlinelibrary.com) DOI: 10.1002/hyp.7958

Quantitative evaluation of different hydrological modelling approaches in a partly glacierized Swiss watershed

Jan Magnusson,[1]* Daniel Farinotti,[2] Tobias Jonas[1] and Mathias Bavay[1]

[1] *WSL Institute for Snow and Avalanche Research SLF, Flüelastrasse 11, CH-7260 Davos Dorf, Switzerland*
[2] *Laboratory of Hydraulics, Hydrology and Glaciology (VAW), ETH Zurich, CH-8092 Zurich, Switzerland*

Abstract:

Mountain water resources management often requires hydrological models that need to handle both snow and ice melt. In this study, we compared two different model types for a partly glacierized watershed in central Switzerland: (1) an energy-balance model primarily designed for snow simulations; and (2) a temperature-index model developed for glacier simulations. The models were forced with data extrapolated from long-term measurement records to mimic the typical input data situation for climate change assessments. By using different methods to distribute precipitation, we also assessed how various snow cover patterns influenced the modelled runoff.

The energy-balance model provided accurate discharge estimations during periods dominated by snow melt, but dropped in performance during the glacier ablation season. The glacier melt rates were sensitive to the modelled snow cover patterns and to the parameterization of turbulent heat fluxes. In contrast, the temperature-index model poorly reproduced snow melt runoff, but provided accurate discharge estimations during the periods dominated by glacier ablation, almost independently of the method used to distribute precipitation. Apparently, the calibration of this model compensated for the inaccurate precipitation input with biased parameters.

Our results show that accurate estimates of snow cover patterns are needed either to correctly constrain the melt parameters of the temperature-index model or to ensure appropriate glacier surface albedos required by the energy-balance model. Thus, particularly when only distant meteorological stations are available, carefully selected input data and efficient extrapolation methods of meteorological variables improve the reliability of runoff simulations in high alpine watersheds.

KEY WORDS snow hydrology; glacier hydrology; energy-balance model; temperature-index model

Received 13 May 2010; Accepted 9 November 2010

INTRODUCTION

Hydrological models of glacio-nival watersheds need to cope with both the melting of snow and ice. At the same time, the melt processes have to be expressed in a distributed way, because the meteorological conditions and the snow and ice cover vary spatially. In previous studies of glacierized watersheds, melt rates have been simulated with either energy-balance or temperature-index models (e.g. Hock, 1999; Hock and Holmgren, 2005; Huss *et al*., 2008b; Michlmayr *et al*., 2008). The two model types show rather similar performance for snow-dominated regions (e.g. Zappa *et al*., 2003; Lehning *et al*., 2006). However, it is still unclear whether detailed energy-balance models or simpler temperature-index melt models developed for both snow and ice produce more reliable predictions of discharge dynamics in watersheds with a glacio-nival runoff regime. Addressing this topic is important for mountain water resources management in the Alps because here watersheds combining both glaciers and snow-dominated areas are rather the rule than the exception.

Hydrological models require meteorological input data often obtained by extrapolating measurements from coarsely distributed weather stations. In mountainous regions, meteorological conditions usually vary greatly over short distances. Therefore, extrapolated weather station data may not fully represent the spatial variations in meteorological driving forces that determine snow and ice melt. Thus, a second important question to address is whether the two melt model types mentioned above have different capabilities in coping with only partly representative input data. This topic gains additional importance when using such models for climate change studies, which typically have to rely on rare meteorological stations providing long-term data records.

In this study, we analysed different discharge modelling approaches in a Swiss glacio-nival watershed under input data constraints typical for long-term simulations, such as climate change assessments. We first assessed different extrapolation schemes of long-term meteorological measurement records using evaluation data from supplementary stations deployed at the study site. In particular, we examined four different methods to distribute solid precipitation. We then compared the performance of a detailed energy-balance and a temperature-index melt model forced with data obtained from the above

* Correspondence to: Jan Magnusson, WSL Institute for Snow and Avalanche Research SLF, Flüelastrasse 11, CH-7260 Davos Dorf, Switzerland. E-mail: magnusson@slf.ch

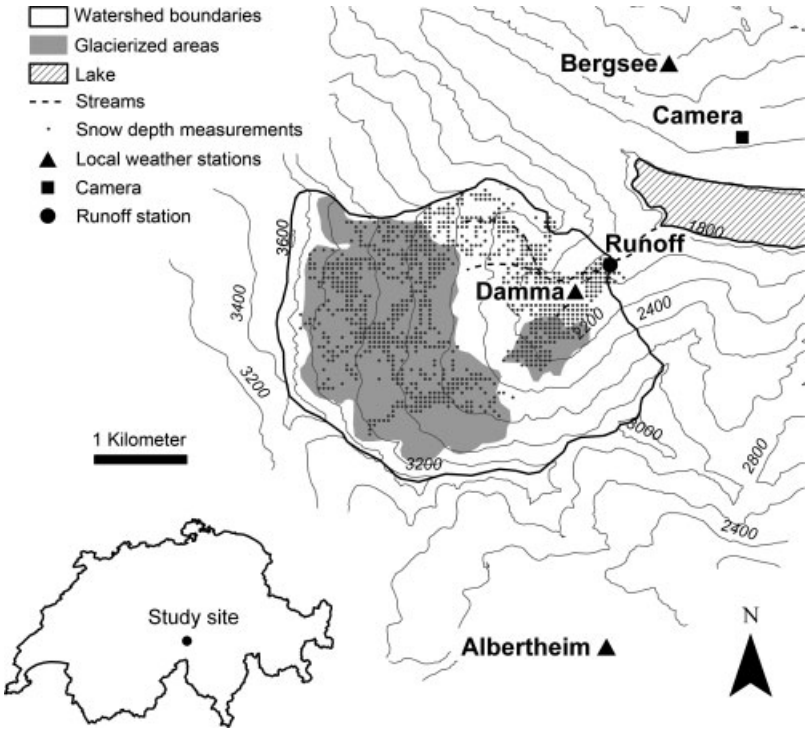

Figure 1. Overview map of the Dammagletscher watershed showing ice-covered regions (grey shaded regions), the local automatic weather stations (triangles), the runoff station (filled circle), the camera (filled rectangle) and the locations of the snow depth measurements averaged to the grid cells of the digital elevation model (dots). Terrain elevation is indicated by 200 m contour lines

mentioned extrapolations of long-term weather station data. The energy-balance model (ALPINE3D) was particularly designed to simulate snow cover dynamics (Lehning *et al*., 2006). The temperature-index melt model, on the other hand, was developed primarily for glacier mass balance modelling studies (Hock, 1999). The four methods to distribute solid precipitation were evaluated through the snow simulations using measured snow water equivalents and snow covered area. To generate a discharge hydrograph, we applied a simple linear reservoir approach for both melt models and evaluated the discharge simulations with measured runoff. Our results show that accurate estimates of snow distribution patterns (i.e. distribution of solid precipitation) are an important prerequisite for reliable prognostic runoff predictions by both models. They are needed either to constrain the melt parameters of the temperature-index model correctly or to ensure appropriate glacier surface albedos required by the physically based model.

STUDY SITE AND DATA

The Damma glacier basin in the central Swiss Alps (N46°38·177′ E08°27·677′) covers an area of 9·9 km^2 and an elevation range from 1940 to 3630 m a.s.l (Figure 1). The hydrological regime of the study area is dominated by runoff generation from the seasonal snow cover and the glacier. The runoff from the basin discharges entirely to a hydropower dam (Göscheneralpsee). The topography of the watershed is characterized by high alpine terrain with steep slopes facing towards the glacier. On the forefield downstream the glacier, a debris-covered dead-ice body constitutes the most prominent feature. The glacier front has receded at an average rate of about 10 m/year since 1921 (Haemmerli *et al*., 2007). A last temporary advance of the glacier front was recorded between 1972 and 1991. The catchment was 50% glacier-covered in 2007. The catchment is underlain by granite bedrock and glacial tills are found on the recently deglacierized parts. The topography of the watershed is known from a high-accuracy digital elevation model obtained by airborne photogrammetry in 2007. For this study, the digital elevation model was resampled to a 50 m grid.

Meteorological measurements from three different station networks were used (Table I): (1) three local weather stations (Figure 1) provided short-term records (up to two hydrological years) of hourly averages of air temperature, relative humidity, wind speed, wind direction, liquid precipitation, snow depth, snow surface temperature, incoming and reflected short-wave radiation as well as incoming long-wave radiation; (2) two meteorological stations of the ANETZ network of the Federal Office of Meteorology and Climatology in Switzerland (MeteoSwiss) provided long-term measurements (i.e. 30 hydrological years) of air temperature, relative humidity, wind speed, wind direction, incoming short-wave radiation as well as liquid and solid precipitation; (3) one station of the MeteoSwiss NIME-network provided long-term daily liquid and solid precipitation measurements. No meteorological measurements were recorded on the glacier surface directly. Runoff was measured at a gaging station at the outlet of the watershed (Figure 1).

Table I. Meteorological variables recorded at the stations used in this study

Station	Elevation (m a.s.l)	Distance to basin (km)	Measurement period	Parameters
Local stations				
Damma	2025	—	9·2007–10·2009	TA, RH, VW, DW, P_{rain}, ISWR, RSWR, TSS, HS
Albertheim	2341	3·9	10·2008–10·2009	TA, RH, VW, DW, P_{rain}, ISWR, RSWR, TSS, ILWR, HS
Bergsee	2586	2·6	10·2008–10·2009	TA, RH, VW, DW, P_{rain}, ISWR, RSWR, TSS, HS
Regional stations				
Gütsch (ANETZ)	2283	12·0	1981–2009	TA, RH, VW, DW, *P*, ISWR
Grimsel (ANETZ)	1977	12·3	1989–2009	TA, RH, VW, DW, *P*, ISWR
Göscheneralp (NIME)	1740	3·2	1969–2009	*P*

TA: air temperature; RH: relative humidity; VW: wind velocity; DW: wind direction; P_{rain}: liquid precipitation; P: solid and liquid precipitation; ISWR: incoming short-wave radiation; RSWR: reflected short-wave radiation; TSS: snow surface temperature; ILWR: incoming long-wave radiation; HS: snow depth.

Snow depths and densities were measured on the accessible parts of the drainage basin on four different survey dates (5 May 2008, 15 May 2008, 17 January 2009 and 4 May 2009). Altogether, 2309 snow depth measurements and 7 snow density profiles were collected. For the individual surveys, the point snow depth measurements were averaged to one value for each grid cell of the digital elevation model with 50 m resolution. This procedure resulted in 1317 point snow depth measurements available for evaluation. Snow water equivalents were estimated from the snow depth measurements, in combination with a statistical model for snow density that accounts for snow depth, season and elevation (Jonas *et al*., 2009). The model allows a site-specific snow density offset, which was evaluated from the observed snow densities. The evolution of the snow cover distribution during the spring, summer and autumn months was tracked with photography. Snow covered areas were extracted from the photographs with a method developed by Farinotti *et al*. (2010), where examples of the snow distribution images for the Dammagletscher basin are available. The camera was located about 2 km east from the catchment outlet and the field of view covered 62% of the drainage basin (Figure 1). The ice-thickness distribution for the Dammagletscher presented by Farinotti *et al*. (2009) was adopted in this study.

MODEL DESCRIPTIONS

Energy-balance model

The energy-balance model (ALPINE3D) is a deterministic and distributed model, designed for high-resolution simulations of snow processes in mountainous terrain (Lehning *et al*., 2006). Initially ALPINE3D was not developed for simulations of glacierized basins, but can reproduce glacier melt and accumulation dynamics (Michlmayr *et al*., 2008; Mott *et al*., 2008). It is based on the one-dimensional SNOWPACK model described in detail by Lehning and Fierz (2008) and references therein. The SNOWPACK model simulates the snow pack development by solving the heat and mass transfer equations of the snow cover. The snow micro-structure in individual layers of the snow pack determines the thermal conductivity and viscosity. Phase changes and snow compaction are accounted for in the model. Many validation studies of the model have been published and in our context the simulations by Obleitner and Lehning (2004) of snow and ice development on a glacier is likely the most important. Their study suggests that SNOWPACK should be able to reproduce accumulation areas of glaciers, where aging snow transforms to ice.

The energy-balance at the surface is divided into radiation and turbulent heat flux terms. The radiation distribution in the basin is handled by a radiosity model, which includes arbitrary multiple terrain reflections, solar shadowing, and long-wave irradiance by surrounding terrain (Helbig *et al*., 2009, 2010). Furthermore, the model also distributes incoming radiation over the uppermost snow layers with a density dependent extinction coefficient (Lehning *et al*., 2002). This allows for a more realistic simulation of the surface energy-balance and sub-surface melting. It may be important to note that for an energy- and mass-balance model, ice melt is not different from snow melt, although ice has a lower albedo, which needs to be estimated. The albedo formulation for snow is based on a statistical model developed for seasonal snow in alpine terrain (Lehning *et al*., 2002). The albedo of glacier ice was set to 0·3 (slightly dirty ice) after Paterson (1994). The assumption of a constant albedo of glacier ice has been shown to have minor effects on runoff formation (Hock and Holmgren, 2005). The albedo of snow was limited to values between 0·95 (newly fallen snow) and 0·53 (average firn albedo) following Paterson (1994).

The turbulent heat fluxes of the energy-balance are described by the Monin-Obukhov similarity theory (Lehning *et al*., 2002). The surface fluxes include the latent heat transfer, and therefore surface evaporation and sublimation are modelled. A variety of stability correction functions are now implemented, but can be switched off, which is often a good choice to avoid unrealistic dampening of the turbulent transfer in rough terrain (Stoessel

et al., 2010). How the stability corrections are handled in this study is described in detail below.

For our investigation area, the Dammagletscher, initial simulations showed that the glacier melt rates were largely affected by the formulation of atmospheric stability, especially after melt-out of seasonal snow, that is, for the exposed ice surface. Heuristically, we achieved reasonable glacier melt rates by: (1) assuming neutral stability outside the glacier which means that no stability correction was performed; (2) assuming neutral stability over the glacier if air temperatures were below 5 °C; and (3) applying the implemented stability-correction scheme of Stearns and Weidner (1993) over the glacier if the air temperatures exceeded 5 °C. This choice is reasonable because it has been shown that very often over snow in complex terrain, stability correction functions dampen the turbulent fluxes in an unreasonable way (Martin and Lejeune, 1998) and the assumption of neutral stability shows better results (Stoessel *et al*., 2010). At the same time, a strong stable stratification often develops over the rather smooth ice surface of a melting glacier (Paterson, 1994).

The model is initialized with a digital elevation model (here with 50 m grid resolution), a description of the soil properties, and the ice-thickness distribution of the glacier. The model is driven by hourly measurements of air temperature, relative humidity, wind speed, precipitation and incoming short- and long-wave radiation. In this study, the model separates between snow and rain by a threshold temperature of 1·2 °C. Furthermore, we did not use an ALPINE3D module describing the small scale transport of snow (Lehning *et al*., 2008).

Temperature-index model

The temperature-index model adopted in this study is based on a distributed temperature-index approach proposed by Hock (1999). Hourly snow- and ice-melt rates M_i occurring at any location i are computed according to:

$$M_i = \begin{cases} \left(f_{\mathrm{M}} + r_{\mathrm{snow/ice}} \cdot I_{\mathrm{pot},i}\right) \cdot T_i & \text{if} \quad T_i > 0\,^{\circ}\mathrm{C} \\ 0 & \text{if} \quad T_i \leq 0\,^{\circ}\mathrm{C} \end{cases} \tag{1}$$

where f_{M} is a melt factor, $r_{\mathrm{snow/ice}}$ are two distinct radiation factors for snow and ice, respectively, $I_{\mathrm{pot},i}$ is the potential solar radiation at the location i and T_i is the mean hourly air temperature at the same location. $I_{\mathrm{pot},i}$ is a function of the considered location i, accounting for effects of slope, aspect and shading, and of the day of the year, accounting for the seasonality of incident solar radiation. Values of $I_{\mathrm{pot},i}$ are calculated in hourly timesteps.

Accumulation is calculated from the given precipitation fields by distinguishing solid and liquid precipitation through a threshold temperature of 1·2 °C. Once on the ground, solid precipitation is not further redistributed, as such effects are integrated in the precipitation fields.

The temperature-index model was calibrated exploring the parameter space given by f_{M}, r_{ice} and r_{snow} through Monte Carlo simulation. On the basis of the assumptions that the residence time of the water in the catchment is shorter than 2 weeks and that evaporation and subsurface runoff are negligible, the objective function was defined as the sum of squares of the residuals given as the difference between measured and modelled runoff aggregated over 2 weeks. The match between the observed and modelled melt-out patterns—quantified by the average percentage of catchment area for which the snow cover is reproduced correctly—was used as an additional criterion to judge the model performance.

Runoff routing scheme

In order to assess how the two different melt models and the different methods to distribute precipitation affected the simulated discharges, we examined several simple runoff routing schemes based on the concept of linear storages. In the following, we present results from a model using two reservoirs, one representing the glacierzied areas and one representing the non-glacierzied regions of the watershed. More complicated constellations of reservoirs (e.g. linear storage models as presented by Schaefli *et al*. (2005) and Huss *et al*. (2008b)) did not significantly improve the simulation results. Note that the runoff routing schemes were intentionally not calibrated to match the total observed discharge volume. This approach was used to inhibit the calibration procedure compensating for systematic overestimation of modelled melt rates.

The two recession coefficients were initially calibrated by exploring the parameter space through Monte Carlo simulations. The obtained best parameter set was then locally refined using an unconstrained nonlinear optimization algorithm (Lagarias *et al*., 1998). The squared correlation coefficient between simulated and measured discharge was used as the objective function. If instead the sum of squared errors were used, which is a common choice of objective function, the calibration minimized the objective function by increasing the recession coefficients to unreasonable values whenever the models overestimated discharge during the calibration period.

In this study, the runoff routing scheme was decoupled from the melt models. This is the typical approach for energy-balance models, in which the parameters of the runoff model are calibrated after the melt simulations. The usual method for temperature-index models would be to couple the melt model with the runoff routing scheme and then calibrate the parameters together. We are convinced that our approach is the fairest test for comparing the two melt models. However, the temperature-index model would perhaps show higher performance measures if the complete system, melt model and runoff routing scheme coupled, was calibrated at once.

EXTRAPOLATION OF METEOROLOGICAL MEASUREMENTS

We extrapolated data from weather stations of the ANETZ and NIME networks with long-term records to

Table II. Performance measures of extrapolated meteorological variables for different time resolutions

Parameter	Unit	Time resolution	R^2	Mean error	RMSE
Air temperature	°C	Hour	0·95–0·97	−0·3 to 0·9	1·2–1·9
		Day	0·97–0·99	—	0·8–1·4
Relative humidity	%	Hour	0·67–0·77	−1·2 to 3·4	11·1–11·3
		Day	0·85–0·88	—	5·8–7·7
Wind speed	m/s	Hour	0·01–0·18	−0·5 to 0·8	1·8–3·6
		Day	0·07–0·29	—	1·2–2·7
Long-wave radiation	W/m^2	Hour	0·58	−11·2	34·0
		Day	0·71	—	25·8
Short-wave radiation	W/m^2	Hour	0·87	−9·8	104·2
		Day	0·80	—	47·9
Acc. precipitation	mm	Day	0·42–0·48	−0·50 to −0·16	7·9–9·0
		Three Day	0·57–0·59	−1·50 to −0·48	13·9–15·6

R^2: squared correlation coefficient; Mean error: mean error defined as the average difference between extrapolated and observed record; RMSE: root mean squared error. If several measurements were available for comparison, the range of the performance measures is listed. The performance measures were determined for the complete available data records at the local stations (Table I).

imitate the typical input data situation for hydrometeorological assessments of alpine watersheds. We used data from three stations within the networks, here termed 'regional stations' or 'regional observations' (Table I). The Dammagletscher and the three regional stations were located in the same climatic region defined by Laternser (2002). The measurements at the regional stations were extrapolated to the watershed using different schemes. The performance of the extrapolation schemes was assessed by comparison against the Damma, Bergsee and Albertheim stations (Figure 1), here termed 'local stations' or 'local observations', using the complete available data records (Table I). Note that the stations only cover altitudes below the main glacierized part of the basin and that the reliability of the methods are unknown for the highest regions of the watershed. The temperature-index model requires measurements of precipitation and air temperature. The energy-balance model also requires measurements of relative humidity, wind speed and short- as well as long-wave radiation in addition to these data. As precipitation is an important input variable but at the same time difficult to extrapolate, we tested different distribution schemes. This is why respective methods are presented in a separate section (Section on 'Methods to Distribute Precipitation').

Air temperature

Hourly air temperatures were distributed to the model grid by shifting the measurements from the station Grimsel to the given altitudes using monthly lapse rates. The measurements at Grimsel showed the highest correlation ($R^2 = 0{\cdot}97$) with the local station on the glacier forefield. We determined the monthly temperature lapse rates using the two stations Grimsel and Gütsch because they showed much higher correlation with our local measurements ($R^2 = 0{\cdot}95$–$0{\cdot}97$, depending on the considered local stations) than the remaining regional stations ($R^2 \leq 0{\cdot}88$). Note also that the two stations Grimsel and Gütsch have a much longer time-series (20 years of data) than the local stations (1 year). The determined lapse rates varied between 0·24 (January) and 0·64 (May) °C/100 m. They showed good agreement with lapse rates determined from the local stations (RMSE $\leq 0{\cdot}07$ °C/100 m).

The extrapolated air temperatures showed a nearly linear relation to the local observations, and the deviations between the records were small (Table II). The statistical performance was similar to that found by Liston and Elder (2006b), who examined a meteorological model for a study area located in North America characterized by moderate topographic relief. Thus, we consider that the extrapolated air temperatures represent the local conditions well. However, note that the local measurements may not be representative for air temperatures on the glacier.

Relative humidity

Relative humidity was distributed using extrapolated air and dewpoint temperatures from the Grimsel station which showed the highest correlation ($R^2 = 0{\cdot}77$) for relative humidity with the local measurements on the glacier forefield. Monthly varying lapse rates were assumed for both air and dewpoint temperature, and determined from measurements recorded at Grimsel and Gütsch (Section on 'Air Temperature'). The dewpoint was calculated using the inverted saturation pressure function presented by Buck (1981) and showed lapse rates between 0·29 (August) and 0·57 (November) °C/100 m. The root mean squared error between these monthly lapse rates and lapse rates determined using the local stations was 0·17 °C/100 m and decreased to 0·07 °C/100 m when omitting the values computed for June and July. The extrapolated air- and dewpoint temperatures were converted back to relative humidities using the function for saturation pressure of Buck (1981).

The extrapolated relative humidities were highly correlated to the local measurements with relatively small errors (Table II). As for air temperature, the statistical performance was similar to that found by Liston and Elder (2006b). However, we again have to restrain

the finding to non-glacierized regions because the local measurements may not be representative for the actual conditions on the glacier.

Wind speed

Wind speed is difficult to predict in mountain regions (Ryan, 1977), and wind direction and speed vary greatly over short distances (Ha *et al*., 2009). To extrapolate wind speeds, we simplified the approach presented by Winstral and Marks (2002) and Winstral *et al*. (2009). The method is based on the terrain parameter Sx which indicates whether a grid cell of a digital elevation model is sheltered or exposed towards a specified wind direction. The parameter Sx is given by the maximum slope between the grid cell of interest and the grid cells along a 300 m long line pointing towards a specified wind direction from this grid cell (Winstral and Marks, 2002):

$$Sx(x_i, y_i) = \max\left(\tan^{-1}\left\{\frac{\mathrm{ELEV}(x_v, y_v) - \mathrm{ELEV}(x_i, y_i)}{[(x_v - x_i)^2 + (y_v - y_i)^2]^{0.5}}\right\}\right) \quad (2)$$

where $\mathrm{ELEV}(x_i, y_i)$ is the altitude of the grid cell of interest with coordinates (x_i, y_i), and $\mathrm{ELEV}(x_v, y_v)$ are the elevations of the grid cells with coordinates (x_v, y_v) along the 300 m long line pointing towards the wind direction from the grid cell of interest.

We used the following procedure to extrapolate wind speeds from the reference station Gütsch which showed the highest correlation coefficient ($R^2 = 0{\cdot}14$) with the station on the glacier forefield: (1) the terrain parameter was determined for the reference station Sx_{ref}, the local stations Sx_{local} and the model grid Sx_{grid}. We averaged the terrain parameters for all wind directions determined with 5° increments. The averaging was performed because the terrain modified the observed wind directions greatly; (2) the terrain parameters of the model grid Sx_{grid} were linked to wind speeds at the reference station with a so-called wind factor wf. The dependent wind factor was determined by a linear function with two parameters a and b:

$$wf = a + b \cdot (Sx_{\mathrm{grid}} - Sx_{\mathrm{ref}}) \quad (3)$$

and the difference between the terrain parameters of the model grid and the reference station ($Sx_{\mathrm{grid}} - Sx_{\mathrm{ref}}$) as independent variables; (3) the two parameters of the linear function were determined by regression using the measurements of the local stations and the reference station. The dependent wind factors, here defined as the ratio of the averaged wind speed at the local stations and the reference station ($VW_{\mathrm{local}}/VW_{\mathrm{ref}}$), were plotted against the independent variables, the difference between the terrain parameter of the local stations and the reference station ($Sx_{\mathrm{local}} - Sx_{\mathrm{ref}}$). We used 5 months of data captured during winter for the regression because then the snow covered ground at the different measurement sites had similar surface roughnesses; (4) with the two parameters a and b defined, the wind factors for the model grid could be determined using Equation (3). The wind speeds measured at the reference station were simply multiplied by the wind factors. To avoid unreasonable extrapolated wind speeds, a lower limit of 0·3 and an upper limit of 1·5 were used for the wind factors.

The extrapolated wind speeds correlated poorly with the observations, but the mean errors were, on the other hand, relatively low (Table II). The scatter between the extrapolated and observed wind speeds was larger than in previous studies (Liston and Elder, 2006b; Winstral *et al*., 2009). This may be due to the larger study site and the rougher terrain which considerably modified the observed wind directions. Prior applications of the Sx parameter in smoother terrain were able to sufficiently resolve wind directions and isolate upwind terrain. The inability to resolve local wind direction in this basin goes against the designed usage of the Sx parameter and most likely compromised the results. Thus, our work points to the need for high elevation data from mountain basins, and efficient methods for determining wind directions in highly complex terrains. Furthermore, catabatic winds may also affect the model performance on the glacier. These effects were not examined because measurements on the glacier were unavailable.

Incoming short-wave radiation

The local cloud cover affects the incident solar radiation, an effect difficult to predict from the available ground observations. Therefore, we uniformly extrapolated the measurements from the station Gütsch. The measurements at Gütsch are unaffected by shading from surrounding terrain. The small short-wave radiation dependence on elevation was neglected (Marty *et al*., 2002).

On average, the extrapolated radiation records agreed rather well with the observations at the Bergsee station (Table II). The statistical performance between the extrapolated and observed short-wave radiation was in similar range to that found by Liston and Elder (2006b).

Incoming long-wave radiation

Incoming long-wave radiation was not measured at the regional stations. Instead we predicted long-wave radiation using a parameterization with the extrapolated air temperatures, relative humidities and short-wave radiation as input. The different algorithms summarized and tested for several sites in China and North America by Flerchinger *et al*. (2009) were examined and compared against the observations at the station Bergsee. The clear-sky algorithm of Dilley and O'Brien (1998) combined with the cloud-correction algorithm of Unsworth and Monteith (1975) performed best in reproducing the measurements at Bergsee. The cloud-correction algorithm relies on an estimate of the cloud cover which we obtained by comparing the incoming short-wave radiation with the clear-sky solar radiation following Campbell (1985). See Flerchinger *et al*. (2009) for all the details of the methods used including the procedure to estimate clear-sky solar radiation.

The extrapolated incoming long-wave radiation reproduced the local observations well (Table II). The statistical performance between the extrapolations and observations were similar to that found by Liston and Elder (2006b) and Flerchinger *et al.* (2009). Note that in the study by Flerchinger *et al.* (2009) local data was used as input for parameterizing long-wave radiation whereas we used extrapolated meteorological variables.

METHODS TO DISTRIBUTE PRECIPITATION

By using four different methods to distribute solid precipitation, we examined how various snow cover patterns influenced the runoff simulated by the two melt models. The precipitation fields were generated with hourly measurements from the station Grimsel and scaled on a monthly basis to match the monthly precipitation sums observed at the station Göscheneralp. This scaling was performed because the daily measurements at Göscheneralp showed the highest correlation with the station on the glacier forefield and the smallest errors (Farinotti *et al.*, 2010).

In this study, we attempted to examine how various snow cover patterns influenced the simulated runoff. Therefore, we normalized the precipitation fields against each other to keep the precipitation amounts constant between the four methods. Without this normalization, the different precipitation amounts obtained by the four distribution methods would likely influence the runoff more than the variations in simulated snow cover patterns.

The three first methods represent interpolation schemes typically used when modelling the discharge of glacierized watersheds (Klok *et al.*, 2001; Verbunt *et al.*, 2003; Koboltschnig *et al.*, 2008; Bavay *et al.*, 2009). The fourth scheme includes the effect of snow redistribution and was first presented by Jackson (1994).

P_{unif}—Precipitation was distributed uniformly. The hourly precipitation $P_{\text{unif},i}$ at any location i of the model grid was set equal to the measured precipitation at the station Grimsel. The obtained hourly precipitations were normalized by a factor $\sum P_{\text{grad},i} / \sum P_{\text{unif},i}$ so that the precipitation amounts equalled the results of the second method P_{grad}.

P_{grad}—Precipitation increased linearly with altitude (Peck and Brown, 1962). The hourly precipitation $P_{\text{grad},i}$ was determined by shifting the measured precipitation P_{grimsel} on elevation z_{grimsel} to any altitude z_i in the watershed using a constant lapse rate $\mathrm{d}P/\mathrm{d}z$:

$$P_{\text{grad},i} = P_{\text{grimsel}} + P_{\text{grimsel}} \cdot (z_i - z_{\text{grimsel}}) \cdot \mathrm{d}P/\mathrm{d}z \tag{4}$$

For solid precipitation, we used a lapse rate of 5%/100 m determined from regional measurements and local observations inferred from time-lapse photography (Farinotti *et al.*, 2010).

P_{prism}—Large-scale horizontal precipitation field combined with the gradient precipitation field. The hourly precipitation $P_{\text{prism},i}$ was obtained by multiplying the results from the method P_{grad} by a location-dependent factor $D_{\text{prism},i}$:

$$P_{\text{prism},i} = P_{\text{grad},i} \cdot D_{\text{prism},i} \tag{5}$$

The factor $D_{\text{prism},i}$ was determined by interpolating the gridded PRISM dataset, which describes the mean precipitation distribution throughout the European Alps for the period 1961–1990 (Schwarb *et al.*, 2001), to our model grid. With this method, more precipitation falls in the western parts of the watershed than in the eastern regions. The hourly precipitations were normalized by a factor $\sum P_{\text{grad},i} / \sum P_{\text{prism},i}$.

P_{distr}—Snow redistribution was accounted for with a parametric approach (Huss *et al.*, 2008a). The hourly precipitation $P_{\text{distr},i}$ was determined by multiplying the precipitation obtained by the method P_{grad} with a location-dependent factor $D_{\text{distr},i}$:

$$P_{\text{distr},i} = P_{\text{grad},i} \cdot D_{\text{distr},i} \tag{6}$$

The location-dependent factor $D_{\text{distr},i}$ was calculated in two steps following Huss *et al.* (2008a). In the first step, we linearly increased the factor between 0·5 (most convex-shaped terrain features) to 1·5 (most concave-shaped terrain features) on the basis of curvatures determined from the digital elevation model describing the watershed. In the second step, we linearly decreased the obtained factors from 100% to 0% for surface slope angles between 40° and 60°. Thus, solid precipitation is transferred from the steeper to the flatter regions of the watershed with more deposition in valleys than on ridges. We again multiplied the precipitations by a factor $\sum P_{\text{grad},i} / \sum P_{\text{distr},i}$ to keep the total precipitation constant between the methods.

Liquid precipitation was distributed uniformly with the measurements from Grimsel again scaled on a monthly basis to match the precipitation sums observed at Göscheneralp. We neglected the influence of horizontal variations in liquid precipitation. The regional stations also showed no increase in liquid precipitation with altitude during summer.

The mean error between the daily precipitation sums obtained by the method P_{grad} and the local measurements ranged from −0·16 to −0·5 mm/day at the Damma and Albertheim stations (Table II). This corresponds to an underestimation of the yearly precipitation sums of between 3% and 10%. The yearly precipitation records at the two local stations were determined by combining: (1) the liquid precipitation measurements of the unheated rain gauge; and (2) an estimate of solid precipitation using the model SNOWPACK (see energy-balance model description) forced with continuous measurements of snow depth, air temperature, relative humidity, wind speed, reflected short-wave radiation and snow

Table III. Evaluation of observed and modelled snow covered area. The simulations driven by the precipitation distribution method accounting for snow redistribution (P_{distr}) matched the observed snow cover patterns more accurately than the remaining simulations

Prec. Method	Period	Energy-balance model			Temperature-index model		
		Match %	Overestimate %	ΔGlacier %	Match %	Overestimate %	ΔGlacier %
P_{unif}	Calibration	76	18	−11	70	27	−1
	Evaluation	75	18	−6	72	23	6
P_{grad}	Calibration	76	18	−6	73	18	−8
	Evaluation	76	16	−3	73	13	−10
P_{prism}	Calibration	76	18	−5	72	22	−1
	Evaluation	76	16	−3	73	17	0
P_{distr}	Calibration	80	13	5	81	11	−2
	Evaluation	81	9	3	80	6	−7

Match: the percentage of matching grid cells between the observation and simulation $(Sim_{snow} \cap Obs_{snow}) \cup (Sim_{snowfree} \cap Obs_{snowfree})$ averaged over the observation period; Overestimate: the overestimation of snow covered area by the simulation compared to the observation $(Sim_{snow} \cap Obs_{snowfree}) - (Sim_{snowfree} \cap Obs_{snow})$ averaged over the observation period; ΔGlacier: difference between simulated and observed snow cover area on the glacier at the end of the summer (in percentage of glacierized area). For the calibration period, 10 photos were available taken on regular intervals during the period from 23 May 2008 to 21 August 2008. For the evaluation period, six photos were available taken on regular intervals during the period from 30 May 2009 to 1 August 2009.

surface temperature. Note that manual snow depth measurements showed no indications of snow redistribution around the stations. Further, the mean errors between the extrapolated and local precipitation records were below the uncertainties of the precipitation estimates from the SNOWPACK model (Egli *et al*., 2009). Therefore, we consider that the P_{grad} method reproduces the precipitation sums for the two local stations well. However, we recognize that the yearly precipitation falling within the watershed may deviate from those obtained by our precipitation fields.

The extrapolated hourly precipitation records of the P_{grad} method correlated poorly with the local observations ($R^2 \leq 0{\cdot}21$). Thus, large runoff events driven by short precipitation events might not be captured adequately by hydrological models forced with the precipitation fields. The daily and three-daily precipitation sums showed significantly higher correlations with the observations than the hourly records.

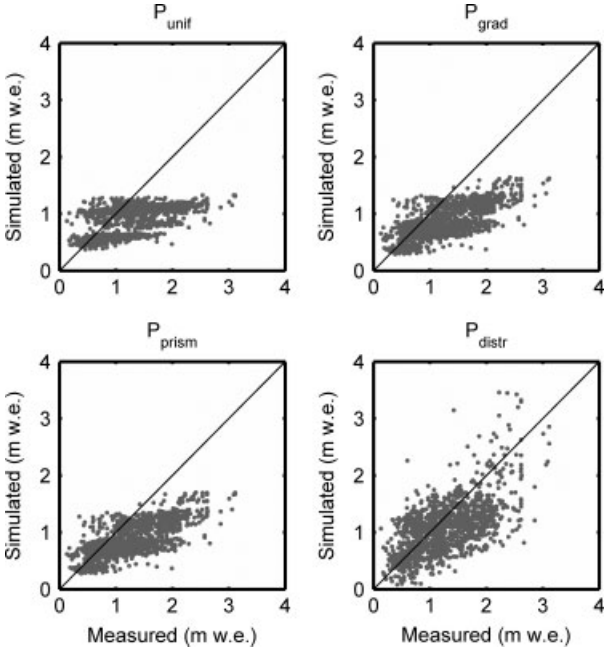

Figure 2. Scatter plots with measured and simulated snow water equivalents (in meters water equivalent) for the four precipitation distribution methods (P_{unif}, P_{grad}, P_{prism} and P_{distr}). The plots show the energy-balance model results. The temperature-index model results were similar. The simulations driven by the precipitation distribution method including snow redistribution (P_{distr}) reproduced the observed snow water equivalents roughly, whereas the other simulations showed no relationship between model results and observations

RESULTS OF SNOW COVER SIMULATIONS

The model results showed that the precipitation distribution method including snow redistribution (P_{distr}) most accurately reproduced the measured snow covered area and snow water equivalents. With these precipitation fields the simulated snow cover area matched the observations best (Table III) and adequately reproduced the accumulation area of the glacier late in summer (Figure 3). These simulations also captured the variability of observed snow water equivalents decently (Figure 2) with a relatively low mean error between the observations and simulations (0·15 m w.e.). This indicates that the total winter precipitation was accurately modelled. However, the last comparison is rather uncertain partly because the observed snow water equivalents were determined using a statistical model of snow densities which was accurate within 17% from the observed snow densities. The comparison between point measurements and gridded model outputs also introduces further uncertainties.

For the simulations driven by the precipitation distributions not accounting for snow redistribution (P_{unif}, P_{grad} and P_{prism}), the steep slopes in the western part of the watershed remained snow covered during the summer and the accumulation area of the glacier was not reproduced correctly (Figure 3). These simulations also displayed much lower variability of snow water equivalents than what was observed in field (Figure 2). We

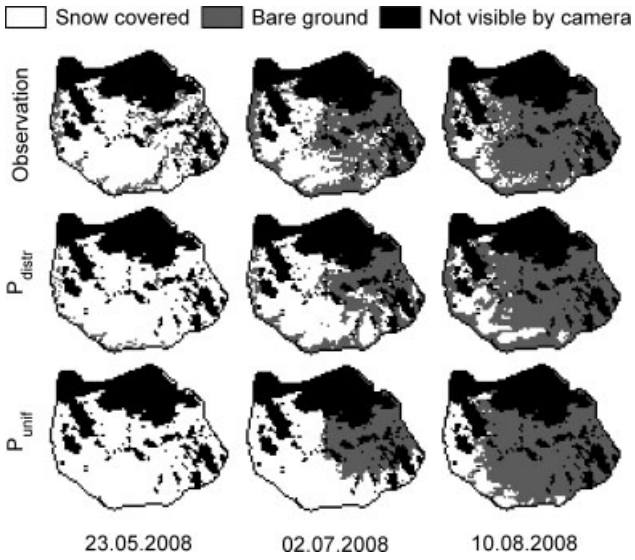

Figure 3. Observed snow covered area and simulated based on the P_{distr} and P_{unif} precipitation fields. The images show the energy-balance model results, which did not differ significantly from the temperature-index model results. Results of the P_{grad} and P_{prism} precipitation distribution methods are similar to the simulations driven by the P_{unif} precipitation fields. White regions are covered by snow. Grey regions are snow free. The black regions were not visible by the camera. The simulations forced by the precipitation distribution method accounting for snow redistribution (P_{distr}) reproduced the accumulation areas of the glacier correctly. The steep slopes in the western part of the watershed remained snow covered during the summer for the remaining simulations instead

conclude that the parametric approach to distribute precipitation improves the snow cover simulations significantly.

RESULTS OF RUNOFF SIMULATIONS

In the following, we present results where we used the discharge measurements from 2008 for calibration and the measurements from 2009 for evaluation. The results of switching the calibration and evaluation periods are not shown, but are similar to the results reported here. In 2008, data from June to December were available (178 days). In 2009, data from March to October were available (214 days).

Influence of precipitation distribution on simulated runoff by the energy-balance model

The runoff simulations by the energy-balance model were sensitive to the different precipitation distributions (Table IV). The simulations driven by the precipitation fields accounting for snow redistribution (P_{distr}) reasonably captured the observed runoff. The total simulated discharge was close to the observations, deviating by only 11 mm ($\leq$1%) during the calibration period and 79 mm (3%) during the evaluation period. The simulations forced by the precipitation fields not including snow redistribution deviated largely from the observations. The total simulated discharge differed up to 228 mm (10%) during the calibration period and 349 mm (15%) during the evaluation period from the observations. The simulations driven by uniformly distributed precipitation (P_{unif}) performed worse than the simulations forced by the fields including elevation and horizontal gradients in precipitation (P_{grad} and P_{prism}).

The P_{distr} method displayed lower streamflows than the other precipitation distribution methods (Figures 4 and 5) particularly during periods dominated by ice melt. The comparison between simulated and measured snow covered area in late summer showed that larger regions of the glacier were snow covered for the simulations forced by the P_{distr} method than the remaining precipitation distribution methods (Table III). Thus, the snow cover patterns on the glacier largely affected the simulated discharge due to albedo effects.

In this study, the total discharge varied by $\leq$12% when comparing the four simulations driven by the different precipitation fields. This result is similar to the findings by Dadic *et al*. (2008), where the discharge of the catchment decreased by 22% if gravitational snow transport was modelled. Furthermore, as found in earlier studies, we observed that the results of physically based

Table IV. Performance measures of runoff simulations by the energy-balance model and the temperature-index model. The statistical performance of the simulations by the energy-balance model increased (lower ΔQ and higher NS-efficiency) when more realistic precipitation fields were used (P_{distr}), whereas no such improvement was observed for the simulations by the temperature-index model

Prec. Method	Period	Energy-balance model				Temperature-index model			
		ΔQ	NS	Slope	Intercept	ΔQ	NS	Slope	Intercept
P_{unif}	Calibration	228	0·76	1·06	0·023	18	0·84	0·83	0·100
	Evaluation	349	0·49	1·18	−0·021	145	0·70	0·81	0·170
P_{grad}	Calibration	149	0·76	1·03	0·019	47	0·85	0·85	0·094
	Evaluation	277	0·54	1·14	−0·018	208	0·66	0·82	0·187
P_{prism}	Calibration	128	0·76	1·02	0·019	−53	0·85	0·81	0·091
	Evaluation	256	0·55	1·13	−0·015	78	0·70	0·78	0·173
P_{distr}	Calibration	11	0·79	0·96	0·026	47	0·85	0·82	0·107
	Evaluation	79	0·64	1·04	−0·003	195	0·66	0·78	0·208

ΔQ: difference between the simulated and observed total discharge covering the calibration period (June 2008 to December 2008) and evaluation period (March 2009 to October 2009) in mm; NS: Nash–Sutcliffe efficiency; Slope: slope of linear regression curve between simulated and observed discharge; Intercept: intercept of linear regression curve between simulated and observed discharge (mm/h).

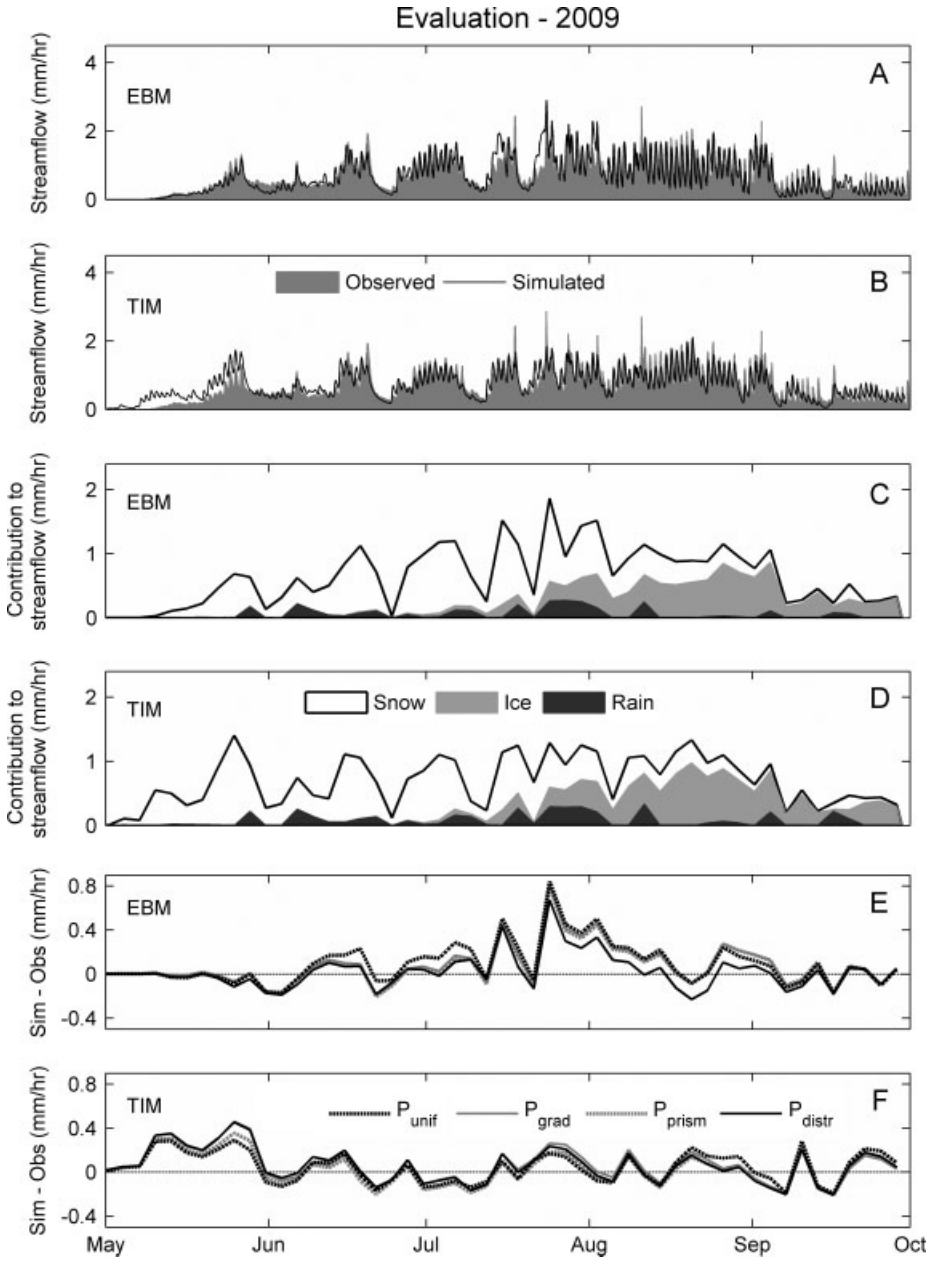

Figure 4. Simulated hourly runoff using the P_{distr} precipitation fields compared with the observed discharge (A and B) for the evaluation period (2009). Three-day averages of simulated water contributing to discharge of liquid precipitation, snow melt and glacier melt based on the P_{distr} precipitation distribution method (C and D). Three-day aggregated residuals, the difference between simulated and observed runoff (E and F). The temperature-index model simulated higher streamflows than the energy-balance model during snow melt, whereas the opposite during glacier melt

snow cover models yield reasonable results provided that they are forced with accurate meteorological data (Winstral and Marks, 2002; Liston and Elder, 2006a).

Influence of precipitation distribution on simulated runoff by the temperature-index model

The runoff simulations by the temperature-index model were rather insensitive to the differently accurate precipitation inputs (Table IV). During the calibration period, the total simulated discharge was close to the observations deviating from the measurements by between −53 (−2%) and 47 mm (2%) depending on precipitation distribution. The deviation increased for the evaluation period to between 78 (3%) and 208 mm (9%), again depending on the method to distribute precipitation. The increasing deviation between simulated and observed total discharge from the calibration to evaluation period might indicate that the calibration parameters of the temperature-index model were non-stationary between the periods. The precipitation distribution method including snow redistribution did not improve the simulation results.

Figures 4 and 5 show that the simulations driven by the four methods to distribute precipitation behaved similarly during the complete calibration and evaluation period. The differences between simulated and observed runoff for the three-day average values varied slightly between the four simulations.

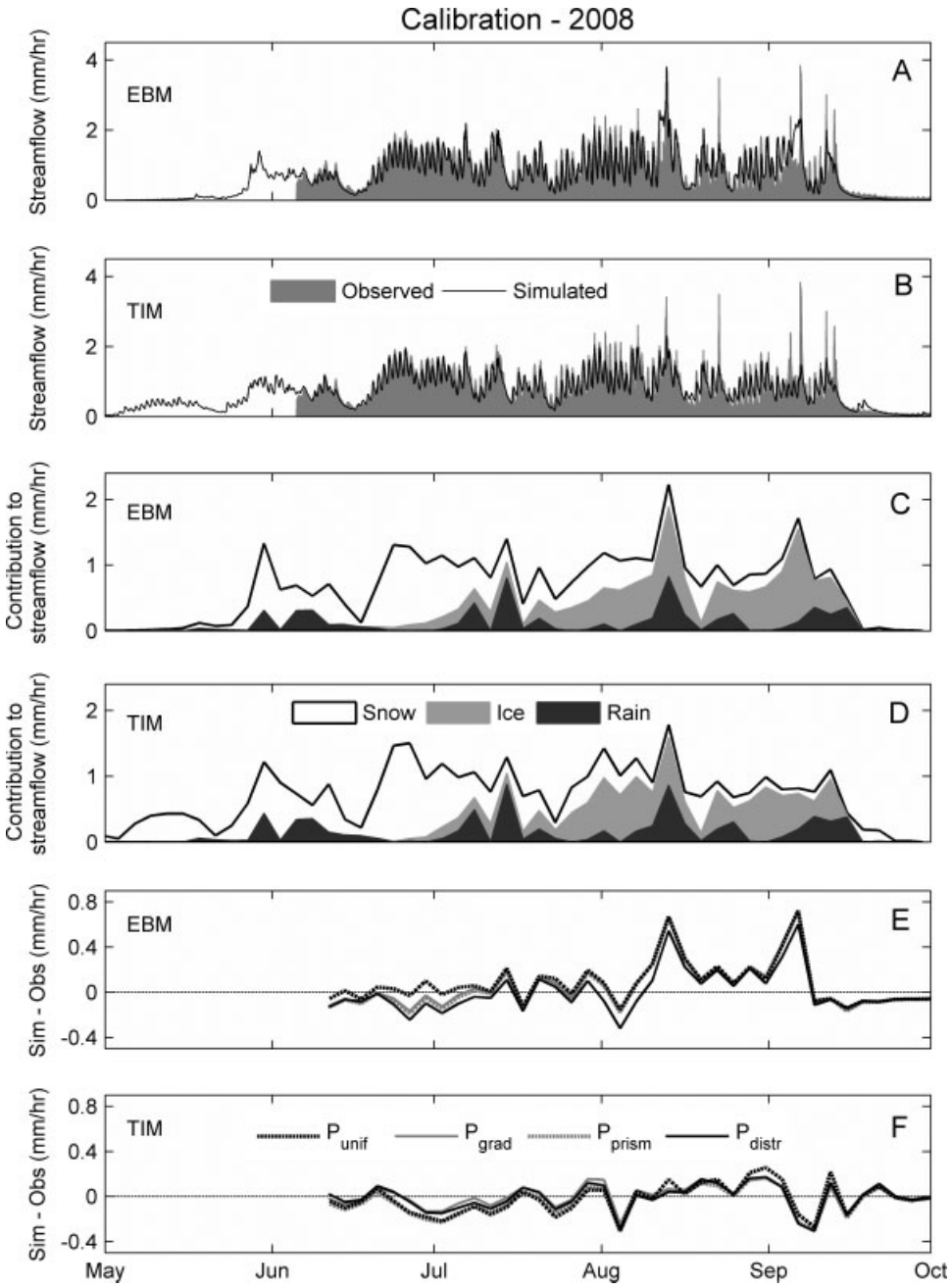

Figure 5. Simulated hourly runoff using the P_{distr} precipitation fields compared with the observed discharge (A and B) for the calibration period (2008). Three-day averages of simulated water contributing to discharge of liquid precipitation, snow melt and glacier melt based on the P_{distr} precipitation distribution method (C and D). Three-day aggregated residuals, the difference between simulated and observed runoff (E and F). The temperature-index model simulated higher streamflows than the energy-balance model during snow melt, whereas the opposite during glacier melt

We conclude that the calibrated melt parameters were able to compensate for inaccuracies in the precipitation fields. Similar compensating mechanisms have been shown in parametric runoff models, and can be considered as a flexible feature of the model to nowcast discharge in spite of inaccurate inputs (Thorne and Woo, 2006). On the other hand, this study also implies that it is difficult to identify whether inappropriate input data may have caused biased parameters through calibration. We therefore suggest that both the simulated discharge and the model input data are validated against measurements. It is also important to note that the parameter values, which were obtained by calibration using short data records, may not be valid over longer periods as they might change with time. To increase the reliability of long-term simulations with temperature-index models (particularly climate change assessments), we would recommend to at least include estimates of the parameter uncertainty following, for example, the methods proposed by Beven (2009).

Runoff simulations reproducing snow melt

The energy-balance model reproduced the snow melt dominated runoff period more accurately than the temperature-index model during the evaluation period (Figure 4). In May, during the first phase of snow

melt the temperature-index model produced considerably higher streamflows than the energy-balance model and the observations. The differences between runoffs simulated by the temperature-index model and the observations were up to 0·45 mm/h averaged over three-day intervals during this period. In 2008, runoff measurements were not available during the same period for comparison. However, the temperature-index model produced higher streamflows than the energy-balance model in this period too (Figure 5). There are at least two possible reasons why the model shows this behaviour. First, the processes of refreezing and percolation of melt water within the snow pack are not included in the temperature-index model, and therefore snow melt may be released too early instead of being retained in the snow pack. Second, the calibration period does not include the complete snow melt period, which may decrease the temperature-index model performance and shows the importance of using an appropriate runoff record for calibration.

Runoff simulations reproducing glacier melt

The temperature-index model reproduced the glacier melt dominated runoff period more precisely than the energy-balance model (Figures 4 and 5). During the period from July to October the temperature-index model displayed smaller deviations from the observations than the energy-balance model for the three-day average values. The largest discrepancies (about 0·84 mm/h) occurred when the sensible heat fluxes on the glacier simulated by energy-balance model exceeded 200 W/m^2. Observations of sensible heat fluxes over alpine glaciers rarely reach these high values (Oerlemans and Grisogono, 2002).

It was impossible to distinguish whether the formulation of the turbulent heat fluxes was inappropriate or if air temperature, relative humidity or wind speed were wrongly extrapolated to the glacier, as direct measurements on the glacier were unavailable. However, the melt rates simulated by energy-balance model were highly sensitive to the assumption of atmospheric stability for the turbulent heat fluxes.

In order to examine the sensitivity of the applied atmospheric stability, two model simulations were performed with the P_{distr} precipitation fields. First, we used a neutral atmosphere over the complete watershed. This resulted in an overestimation of the discharge by 820 mm (35%) for the calibration period covering 178 days and 891 mm (38%) for the evaluation period covering 214 days. Second, we applied a stability correction scheme following Stearns and Weidner (1993). This resulted in an underestimation of discharge by −434 mm (−18%) for the calibration period and −350 mm (−15%) for the evaluation period. Thus, the variable stability correction scheme (see the description of the energy-balance model) was motivated by the following considerations: (1) that the atmospheric stability is mostly neutral over melting snow (Lehning *et al*., 2002); and (2) that the atmospheric stability is often stable over a melting glacier surface (Paterson, 1994).

Statistical performance of runoff simulations

The models displayed similar statistical performances (Table IV) provided that they were forced with the precipitation distribution method including snow redistribution (P_{distr}). Then the Nash–Sutcliffe efficiencies and squared correlation coefficients were comparable between the models. During both the calibration and evaluation period, both models reproduced the total observed runoff within 8%. Thus, both models reproduced the observed discharge with similar statistical performance as found in studies where the input data was measured in the watershed itself (Zappa *et al*., 2003; Hock and Holmgren, 2005; Michlmayr *et al*., 2008).

The slope and intercept of the linear regression between simulated and observed discharge differed between the both models (Table IV). The temperature-index model displayed a flatter slope with a higher intercept than the energy-balance model. This indicates that fast discharge fluctuations were underestimated which suggest that over short time scales the melt rates might be influenced by single energy-balance terms not included in the model. Indeed, this is a known weakness of this model type (Huss *et al*., 2008a). However, fast discharge fluctuations are also largely influenced by the parameters of the runoff routing scheme. The decoupling of the runoff routing model from the melt model during calibration might also influence the performance of the temperature-index model.

CONCLUSIONS

We evaluated an energy-balance model with focus on snow processes and a temperature-index model designed for glacier mass balance studies in a watershed with glacio-nival runoff regime. The models were forced with data extrapolated from long-term measurement records to mimic the typical input data situation for climate change assessments. In general, the extrapolation schemes of the necessary model input variables accurately reproduced the local observations covering the lower elevation ranges at the study site. In particular, the method to distribute precipitation including snow redistribution effects (P_{dist}) improved the snow cover simulations. However, hourly variations in precipitation and wind speed were not captured correctly by the applied extrapolation schemes. This may be an explanation why the models forced with these data occasionally failed to capture short-term runoff events. This study shows the importance of distributed meteorological measurements at higher elevations, which are needed to improve extrapolation schemes providing input data to hydrological models of alpine basins.

The runoff simulations by the detailed energy-balance model were accurate during the snow melt dominated

period of the year, but dropped in performance during the glacier ablation season. For more reliable prediction of glacier melt, further studies with direct measurements on the glacier are needed in order to validate the input data and the contributions of single energy-balance terms to melting (i.e. turbulent heat fluxes and radiation budget). The snow distribution largely influenced the runoff simulations, mainly by affecting the glacier albedo. The results indicate that the simple method to distribute precipitation including snow redistribution effects may be an efficient method to ensure more accurate simulations of the average glacier albedo.

The temperature-index model properly reproduced the observed runoff during the glacier ablation season. However, during the snow melt dominated period of the year the runoff was considerably overestimated. The reason for this behaviour may be that the model neglects refreezing and percolation of melt water in the snow pack or that the runoff record used for calibration did not include the snow melt period. If the second explanation is correct, our results show the importance of using an appropriate runoff record for calibration. The model performance was independent of the precipitation distribution, showing that the calibration of the model compensated for inaccurate forcing fields.

We conclude that thorough input data pre-processing facilitates accurate runoff estimations in alpine watershed, especially if model input data need to be extrapolated from distant meteorological stations. Both model types tested reproduced observed discharge with similarly good statistical performance. However, with individual strengths and weaknesses, the models may be differently suited for specific applications.

ACKNOWLEDGEMENTS

Financial support for this study was provided by the BigLink project of the Competence Center for Environment and Sustainability (CCES) of the ETH Domain. Many students and staff, particularly B. Fritschi and K. Steinier, helped with the field work and deserve gratitude. Many thanks to M. Lehning, who helped with the modelling. Finally, we acknowledge two reviewers for their helpful remarks.

REFERENCES

Bavay M, Lehning M, Jonas T, Loewe H. 2009. Simulations of future snow cover and discharge in Alpine headwater catchments. *Hydrological Processes* **23**: 95–108.

Beven K. 2009. *Environmental Modelling; An Uncertain Future?* Routledge: London and New York.

Buck AL. 1981. New equations for computing vapor-pressure and enhancement factor. *Journal of Applied Meteorology* **20**(12): 1527–1532.

Campbell GS. 1985. *Soil Physics with Basic: Transport Models for Soil-Plant Systems*, Elsevier: New York.

Dadic R, Corripio JG, Burlando P. 2008. Mass-balance estimates for Haut Glacier d'Arolla, Switzerland, from 2000 to 2006 using DEMs and distributed mass-balance modeling. *Annals of Glaciology* **49**(2): 22–26.

Dilley AC, O'Brien DM. 1998. Estimating downward clear sky long-wave irradiance at the surface from screen temperature and precipitable water. *Quarterly Journal of the Royal Meteorological Society* **124**: 1391–1401.

Egli L, Jonas T, Meister R. 2009. Comparison of different automatic methods for estimating snow water equivalent. *Cold Regions Science and Technology* **57**(2–3): 107–115.

Farinotti D, Huss M, Bauder A, Funk M. 2009. An estimate of the glacier ice volume in the Swiss Alps. *Global and Planetary Change* **68**(3): 225–231.

Farinotti D, Magnusson J, Huss M, Bauder A. 2010. Snow accumulation distribution inferred from time-lapse photography. *Hydrological Processes* **24**: 2087–2097.

Flerchinger GN, Xaio W, Marks D, Sauer TJ, Yu Q. 2009. Comparison of algorithms for incoming atmospheric long-wave radiation. *Water Resources Research* **45**: ARTN W03423.

Ha KJ, Shin SH, Mahrt L. 2009. Spatial variation of the regional wind field with land-sea contrasts and complex topography. *Journal of Applied Meteorology and Climatology* **48**(9): 1929–1939.

Haemmerli A, Waldhuber S, Miniaci C, Zeyer J, Bunge M. 2007. Local expansion and selection of soil bacteria in a glacier forefield. *European Journal of Soil Sciences* **58**(6): 1437–1445.

Helbig N, Loewe H, Lehning M. 2009. Radiosity approach for the shortwave surface radiation balance in complex terrain. *Journal of the Atmospheric Sciences* **66**(9): 2900–2912.

Helbig N, Loewe H, Mayer B, Lehning M. 2010. Explicit validation of a surface shortwave radiation balance model over snow-covered complex terrain. *Journal of Geophysical Research—Atmospheres* **115**: D18113.

Hock R. 1999. A distributed temperature-index ice- and snowmelt model including potential direct solar radiation. *Journal of Glaciology* **45**(149): 101–111.

Hock R, Holmgren B. 2005. A distributed surface energy-balance model for complex topography and its application to Storglaciaren, Sweden. *Journal of Glaciology* **51**(172): 25–36.

Huss M, Bauder A, Funk M, Hock R. 2008a. Determination of the seasonal mass balance of four Alpine glaciers since 1865. *Journal of Geophysical Research-Earth Surface* **113**(F1): ARTN F01015.

Huss M, Farinotti D, Bauder A, Funk M. 2008b. Modelling runoff from highly glacierized alpine catchment basins in a changing climate. *Hydrological Processes* **22**: 3888–3902.

Jackson THR. 1994. A spatially distributed snowmelt-driven hydrological model applied to Upper Sheep Creek. PhD thesis, Utah State University, Logan, Utah.

Jonas T, Marty C, Magnusson J. 2009. Estimating the snow water equivalent from snow depth measurements in the Swiss Alps. *Journal of Hydrology* **378**(1–2): 161–167.

Klok EJ, Jasper K, Roelofsma KP, Gurtz J, Badoux A. 2001. Distributed hydrological modelling of a heavily glaciated Alpine river basin. *Hydrological Sciences Journal—Journal des Sciences Hydrologiques* **46**(4): 553–570.

Koboltschnig GR, Schoener W, Zappa M, Kroisleitner C, Holzmann H. 2008. Runoff modelling of the glacierized Alpine Upper Salzach basin (Austria): multi-criteria result validation. *Hydrological Processes* **22**: 3950–3964.

Lagarias JC, Reeds JA, Wright MH, Wright PE. 1998. Convergence properties of the Nelder-Mead simplex method in low dimensions. *SIAM Journal on Optimization* **9**(1): 112–147.

Laternser M. 2002. Snow and avalanche climatology of Switzerland. PhD thesis, ETH Zürich, dissertation No. 18230.

Lehning M, Fierz C. 2008. Assessment of snow transport in avalanche terrain. *Cold Regions Science and Technology* **51**: 240–252.

Lehning M, Bartelt P, Brown B, Fierz C. 2002. A physical SNOWPACK model for the Swiss avalanche warning. Part III: meteorological forcing, thin layer formation and evaluation. *Cold Regions Science and Technology* **35**(3): 169–184.

Lehning M, Voelksch I, Gustafsson D, Nguyen TA, Staehli M, Zappa M. 2006. ALPINE3D: a detailed model of mountain surface processes and its application to snow hydrology. *Hydrological Processes* **20**: 2111–2128.

Lehning M, Loewe H, Ryser M, Raderschall N. 2008. Inhomogeneous precipitation distribution and snow transport in steep terrain. *Water Resources Research* **44**(7): W07404.

Liston GE, Elder K. 2006a. A distributed snow-evolution modeling system (SnowModel). *Journal of Hydrometeorology* **7**(6): 1259–1276.

Liston GE, Elder K. 2006b. A meteorological distribution system for high-resolution terrestrial modeling (MicroMet). *Journal of Hydrometeorology* **7**(2): 217–234.

Martin E, Lejeune Y. 1998. Turbulent fluxes above the snow surface. *Annals of Glaciology* **26**: 179–183.

Marty C, Philipona R, Frohlich C, Ohmura A. 2002. Altitude dependence of surface radiation fluxes and cloud forcing in the alps: results from the alpine surface radiation budget network. *Theoretical and Applied Climatology* **72**(3–4): 137–155.

Michlmayr G, Lehning M, Koboltschnig G, Holzmann H, Zappa M, Mott R, Schoener W. 2008. Application of the Alpine 3D model for glacier mass balance and glacier runoff studies at Goldbergkees, Austria. *Hydrological Processes* **22**: 3941–3949.

Mott R, Faure F, Lehning M, Loewe H, Hynek B, Michlmayer G, Prokop A, Schoener W. 2008. Simulation of seasonal snow-cover distribution for glacierized sites on Sonnblick, Austria, with Alpine 3D model. *Annals of Glaciology* **49**: 155–160.

Obleitner F, Lehning M. 2004. Measurement and simulation of snow and superimposed ice at the Kongsvegen glacier, Svalbard (Spitzbergen). *Journal of Geophysical Research—Atmospheres* **109**(D4): ARTN D04106.

Oerlemans J, Grisogono B. 2002. Glacier winds and parameterisation of the related surface heat fluxes. *Tellus Series A—Dynamic Meteorology and Oceanography* **54**(5): 440–452. Climate Conference 2001, Utrecht, Netherlands, August, 2001.

Paterson WSB. 1994. *The Physics of Glaciers*, 3rd edn, Pergamon: Oxford.

Peck EL, Brown MJ. 1962. An approach to the development of isohyetal maps for mountainous areas. *Journal of Geophysical Research* **67**: 681–694.

Ryan BC. 1977. Mathematical-model for diagnosis and prediction of surface winds in mountainous terrain. *Journal of Applied Meteorology* **16**(6): 571–584.

Schaefli B, Hingray B, Niggli M, Musy A. 2005. A conceptual glacio-hydrological model for high mountainous catchments. *Hydrology and Earth System Sciences* **9**: 95–109.

Schwarb C, Frei C, Schaer C, Daly M. 2001. Mean annual and seasonal precipitation throughout the European Alps 1971–1990. Hydrological Atlas of Switzerland. Plates 2 · 6, 2 · 7, Technical Report.

Stearns C, Weidner G. 1993. Sensible and latent heat flux estimates in Antarctica. *Antarctic Research Series* **61**: 109–138.

Stoessel F, Guala M, Fierz C, Manes C, Lehning M. 2010. Micrometeorological and morphological observations of surface hoar dynamics on a mountain snow cover. *Water Resources Research* **46**: W04511.

Thorne R, Woo MK. 2006. Efficacy of a hydrologic model in simulating discharge from a large mountainous catchment. *Journal of Hydrology* **330**(1–2): 301–312.

Unsworth MH, Monteith JL. 1975. Long-wave radiation at ground. 1. Angular-distribution of incoming radiation. *Quarterly Journal of the Royal Meteorological Society* **101**(427): 13–24.

Verbunt M, Gurtz J, Jasper K, Lang H, Warmerdam P, Zappa M. 2003. The hydrological role of snow and glaciers in alpine river basins and their distributed modeling. *Journal of Hydrology* **282**(1–4): 36–55.

Winstral A, Marks D. 2002. Simulating wind fields and snow redistribution using terrain-based parameters to model snow accumulation and melt over a semi-arid mountain catchment. *Hydrological Processes* **16**: 3585–3603.

Winstral A, Marks D, Gurney R. 2009. An efficient method for distributing wind speeds over heterogeneous terrain. *Hydrological Processes* **23**(17): 2526–2535.

Zappa M, Pos F, Strasser U, Warmerdam P, Gurtz J. 2003. Seasonal water balance of an Alpine catchment as evaluated by different methods for spatially distributed snowmelt modelling. *Nordic Hydrology* **34**(3): 179–202.

